We are IntechOpen, the world's leading publisher of Open Access books Built by scientists, for scientists

6,900
Open access books available

185,000
International authors and editors

200M
Downloads

Our authors are among the

154
Countries delivered to

TOP 1%
most cited scientists

12.2%
Contributors from top 500 universities



WEB OF SCIENCE™

Selection of our books indexed in the Book Citation Index in Web of Science™ Core Collection (BKCI)

Interested in publishing with us?
Contact book.department@intechopen.com

Numbers displayed above are based on latest data collected.
For more information visit www.intechopen.com



13

Spin Dependent Transport Through a Carbon Nanotube Quantum dot in the Kondo Regime

Stanisław Lipiński and Damian Krychowski
Institute of Molecular Physics, Polish Academy of Sciences
Poznań, Poland

1. Introduction

Carbon nanotubes (CNTs) are thin, hollow cylinders, which can be envisioned as being rolled up from graphene - a two-dimensional honeycomb lattice with a carbon atom in each site. Multiwall carbon nanotubes were discovered by Japanese scientist Sumio Iijima in 1991 (Iijima, 1991) and, two years later, individual single wall carbon nanotubes (SWCNTs) were reported (Iijima & Ichihashi, 1993). Their diameter is as little as 1 nanometer. Carbon nanotubes provide the ultimate limit for microelectronic miniaturization. Soon after discovery carbon nanotubes attracted tremendous interest from fundamental science and technological perspectives and thousands of papers have been published on this subject (for a review see e.g. (Dresselhaus et al., 2001)). Amazing are mechanical properties of CNTs e.g. their high strength and high flexibility. Since the C-C bonds within CNTs are one of the strongest bonds in the nature these tubes are predicted to be by far the strongest fibres that can be made. SWCNT was tested to have tensile strength of order of 60 GPa (Wei, 2003). Nanotubes exhibit also exceptional electrical properties, some of them will be discussed in this chapter. The unique electrical properties of CNTs stem from unusual electronic properties of graphene (Novoselov, 2005; Wallace, 1947). The sp^2 hybridization between one s-orbital and two p-orbitals leads to a trigonal planar structure with a formation of a σ-bond between carbon atoms what is responsible for robustness of the lattice in all carbon allotropes. The unaffected p-orbital, which is perpendicular to the planar structure binds covalently with neighboring carbon atoms leading to the formation of half filled π-bands. The low energy band structure of graphene has two bands that join at the corners of the Brillouin zone (two distinct Fermi points at K and K', called Dirac points (Fig. 1a)). The name of these points reflects the fact that the energy bands disperse linearly away from the touching points, so the dispersion relation for electrons (holes) is described by an isotropic cone that opens upward (downward) near K, K' points (massless fermions). Graphene is a gapless semiconductor. This is changed when rolling up a piece of graphene to form a carbon nanotube. From the bandstructure of graphene one can obtain the bandstructure of nanotube by imposing appropriate boundary conditions along the circumference. Quantization of momentum in the circumferential direction is given by condition $\pi d \cdot k_\perp = 2\pi i$ ($i = 1, 2...$). Spacing in $k_\perp$ is thus $\Delta k_\perp = 2/d$, where d is the diameter of the tube. The quantization cuts discrete slices of two-dimensional Dirac dispersion of graphene. Each line corresponds to a 1D subband for conduction along the nanotube (Fig. 1b, c). Depending on the way graphene is rolled up, carbon nanotube can be either metallic or semiconducting. The former occurs if a slice happens to pass through

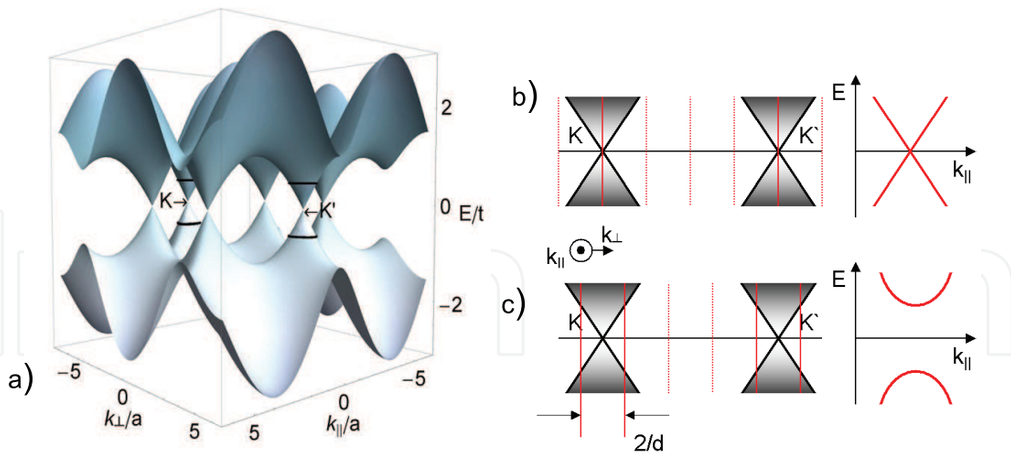


Fig. 1. a) Band structure of graphene. The valence and conduction states meet in K and K' points. b) Quantization of energy in metallic carbon nanotube. The vertical lines represent $k_\perp$ values intercepting the dispersion cones at K and K'. c) Quantization of energy in semiconducting CNT.

the Dirac point (Fig. 1b). Metallic SWNT have a Fermi velocity $v_F \approx 8 \cdot 10^5$ m/s that is comparable to typical metals. Metallic nanotubes have conductivities and current densities that exceed the best metals. Semiconducting SWNTs (Fig. 1c) have a bandgap $E_g \approx 0.9$ eV/d. The inverse dependence of the gap on diameter reflects the similar dependence on diameter of the separation of 1D subbands. Semiconducting tubes have mobilities and transconductances that meet or exceed the best semiconductors.

The research presented in this chapter is addressed to spintronics, a new rapidly developing field of electronics, which exposes the role of spin in controlling current flowing through nanoscopic systems. Spintronic systems have promising potential applications e.g. in reprogrammable logic devices and quantum computing because of long coherent lifetime of spin degree of freedom, fast data processing speed and low dissipation (Das Sarma, 2001). The most spectacular commercial impact of this field to date has been in the area of spin valves used in magnetic hard disk drivers. The principle of operation of such spin valve is based on magnetoresistive effect ($\mathcal{GMR}$), for which the Nobel Prize was awarded in 2007 to Albert Fert and Peter Grünberg. In their experiments it was found (Baibich et al., 1988; Binasch et al., 1989) that the resistivity of non-magnetic spacer layers sandwiched between ferromagnetic films changes unexpectedly largely with the relative alignment of the magnetizations in the films. Later similar effects have been observed in semiconductor tunnel junctions (Tanaka et al., 2001) and molecular systems (Xiong et al., 2004) and the term tunnel magnetoresistance ($\mathcal{TMR}$) has been coined. In this case transport from one ferromagnetic electrode to another occurs not by simple extended state conduction, but by quantum tunneling across a non-magnetic region. In this context, carbon nanotubes are particularly interesting, because they exhibit long spin lifetime and can be contacted with ferromagnetic materials (Cottet et al., 2006). Electronic transport through a nanotube depends on the contacts with electrodes. At low temperatures the properties of short tubes weakly coupled with electrodes are dominated by strong correlations. Of special interest in this respect is Kondo effect - a formation of many-body dynamical singlet between a localized spin and delocalized conduction electrons of electrodes (Hewson, 1993). The tunability of nanostructures have allowed studies of Kondo effect in nonequilibrium. Since carbon

nanotubes posses in addition to spin also orbital degeneracy, it becomes possible to realize in these systems highly symmetric Kondo effect, where both spin and orbital pseudospin are quenched. The increase of degeneracy corresponds to enhancement of Kondo temperature, what is important for potential applications. In the following, we will discuss an impact of symmetry-breaking perturbations in CNTs in the Kondo regime on transport, in specific we will focus on the influence of magnetic field and polarizations of electrodes. The conclusions drawn in this chapter can be easily adopted also to the case of manipulating of orbital degrees of freedom (orbitronics).

2. Carbon nanotube quantum dot

When two metallic electrodes are deposited on top of a CNT, tunnel barriers develop at the nanotube-metal interfaces (Fig. 2). When the resistance of the two barriers becomes comparable to or is larger than the quantum resistance ($R_Q = h/(2e^2)$), the island becomes strongly separated. A finite length L between the electrodes results in quantized of energy levels $\Delta E = (h v_F)/2L$. Discrete level structure is a consequence of quantum confinement effect. Carbon nanotube quantum dot (CNT-QD) is a zero-dimensional island tunnel-coupled to metal leads. Schematic side view of CNT-QD is presented on Fig. 2. With the nanotube

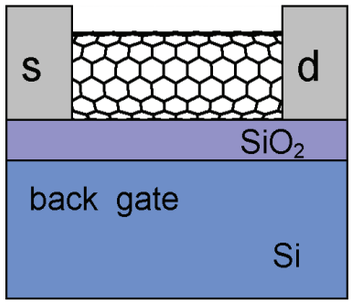


Fig. 2. Schematic side view of carbon nanotube quantum dot.

lying on an oxidized Si substrate, a natural way of gating quantum dot is to apply a voltage to the doped Si. The Si then acts as a back gate affecting the whole dot. For small dots the charging energy $E_C = e^2/(2C)$ becomes important, because the dots have very small capacitances (capacitance of a tube $C/L \sim ln(1/d)$). A typical diameter of SWCNT is $d \sim 1$ nm and L is of order of few hundreds of nm, what gives E_C of order of a few meV. Of the same order, but usually larger is single particle level spacing ΔE ($\Delta E \sim 1.7$ meV/L[μm]). The transmission of the contacts determines the relevant regime for charge transport. Depending on the ratio between tunnel induced broadening of energy levels Γ and charging energy E_C, three regimes can be distinguished:

1. $\Gamma \ll E_C$ - closed QD, charging effects dominate transport (Coulomb blockade regime)
2. $\Gamma \leq E_C$ - intermediate coupling , increasing role of higher order tunneling processes (Kondo regime)
3. $\Gamma \gg E_C$ - open QD, interaction effects do not play the role and transport is dominated by interference (Fabry-Perot regime)

In the first regime for temperatures lower than charging energy the electrons will enter the dot one by one yielding the well known Coulomb blockade (CB) oscillations of the transport as a function of gate voltage V_g (Fig. 3b). The addition of each extra electron to the dot

requires charging energy. This leads to a ladder of discrete addition levels $\mu(N)$ indicating the energy required to add the Nth electron. The Coulomb blockade can be lifted by changing

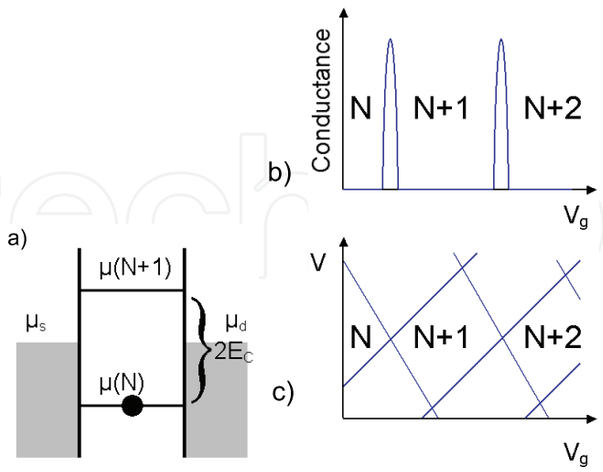


Fig. 3. a) Energy diagram for a quantum dot b) Coulomb oscillations of conductance versus gate voltage. On the peak the number of electrons can fluctuate between N and $N+1$, in between transport is blocked. c) Coulomb diamonds in the differential conductance versus transport voltage and gate voltage.

the gate voltage or by changing the source-drain voltage V (Fig. 3c). In the V_g -V-plane the diamond-shaped regions are observed, in which current is blocked. In a wider range of gate voltage than the one presented on Fig. 3b, apart from charging energy also single particle level spacing separation can be extracted from a nonuniform distribution of conductance peaks. In general the distance between the CB peaks is determined by a sum of charging and quantum confinement energy. In an ideal semiconducting nanotube, sets of four electronic states can be grouped together into a shell. All four states are degenerate, with two choices for spin and two for orbital. The orbital degeneracy can be intuitively viewed to originate from two equivalent ways electrons can circle the graphene cylinder, that is clockwise and anticlockwise. For semiconducting tubes the fourfold periodicity of addition energy is observed (Buitelaar et al., 2002; Liang et al., 2002) and for metallic tubes, where only spin degeneracy is present, twofold shell filling was reported (Cobden & Nygård, 2002). Transport in regime 1 is governed by sequential tunneling (first order tunneling processes), which gives rise to current only at the Coulomb peaks. In the opposite limit of high transparency (regime 3) nanotube acts as an electron wave guide creating resonances at certain energies. Such system can be regarded as an open quantum dot with resonances corresponding to the broad energy levels of the dot (Liang et al., 2001). In the intermediate regime (2) electron number on the dot is still fixed, but significant cotuneling is allowed leading to finite conductance in the valleys between Coulomb peaks (Kondo effect).

3. Exotic spin-orbital Kondo effect

Kondo effect was first discovered in noble metals containing a small concentration of magnetic impurities, where a logarithmic increase of resistivity was observed at low temperatures (de Hass et al., 1933). It was explained by Japanese theorist Jun Kondo in 1964 (Kondo, 1964). Magnetic impurities embedded in metallic hosts cause anomalous resonant scattering of conduction electrons. The many-body dynamical singlet between a localized spin and

delocalized conduction electrons is formed. This effect has become one of the most extensively

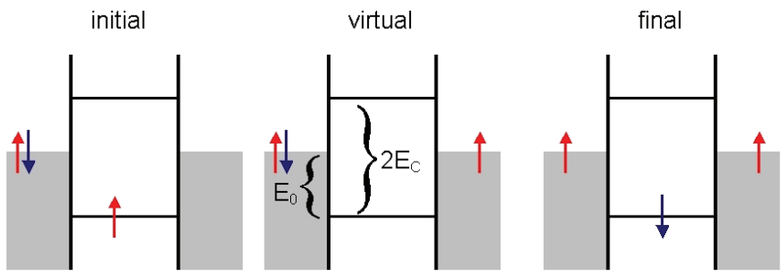


Fig. 4. Spin-flip cotunneling. By going through the different states, the dot spin can effectively be flipped.

studied many body problems in the field of theoretical solid state physics in the last decades. Kondo effect has been also observed in a wide range of nanoscopic systems including semiconductor-based QDs (Cronewett et al., 1998; Goldhaber-Gordon et al., 1998) and molecular systems (Liang et al., 2002; Park et al., 2002). Thanks to versatility of nanoobjects this effect can be studied in a variety of situations, offering quite novel physics. A path of studying this many-body phenomenon in a controlled way and in out-of equilibrium situations has been opened (De Franceschi et al., 2002; Grobis et al., 2008; Paaske et al., 2006). Due to different geometry of QDs coupled to the leads compared to geometry of impurity in an alloy, instead of logarithmic increase of resistance at low temperatures, for QDs a similar increase of conductance is observed. In a quantum dot all electrons have to travel through the device as there is no path around it. Kondo resonance formed at the Fermi energy mixes the states from both leads increasing the conductance. The essence of the Kondo spin screening process in QD is illustrated on Fig. 4, where the spin flip (exchange) cotuneling process is presented. The virtual spin flips at the dot are caused by tunneling processes off the dot with a given spin followed by tunneling of electron of opposite spin on the dot. Classically these processes are forbidden by energy conservation. The intermediate virtual state (Fig. 4) is allowed to exist for a very short time $t \sim h/E_0$ by Heisenberg uncertainty principle. The final state has the same energy as the initial and the sequence of processes shown on Fig. 4 is known as elastic cotunneling (Averin et al., 1992). Adding many spin-flips processes of higher order coherently, the spin-flip rate diverges. The spin-flip processes resonantly enhance around a characteristic temperature called Kondo temperature T_K and change the energy spectrum of the system generating at the Fermi energy many-body resonance known as Kondo resonance. A consequence of its occurrence is an earlier mentioned logarithmic increase of the conductance and its saturation, in the case of symmetric coupling to the leads conductance reaches value $(2e^2)/h$. Electrons are transmitted perfectly through the dot due to location of Kondo resonance at the Fermi energy (Fig. 6). The Kondo temperature sets the temperature, respectively the voltage or magnetic field scale above which the Kondo resonance is suppressed. T_K can be estimated from the width of the Kondo resonance and deduced from the temperature dependence of linear conductance. The Kondo effect can also occur replacing the spin by orbital (Sasaki et al., 2004) or charge (Holleitner et al., 2004; Wilhelm et al., 2002) degrees of freedom. The necessary condition for the occurrence of this effect is the same degeneracy of the states in the electrodes and in the QD and conservation of spin or pseudospin in tunneling processes. For the two-fold degenerate states the allowed symmetry operations are rotations in spin space (SU(2)). Spin and orbital degeneracies can also occur simultaneously leading to highly symmetric Kondo state (SU(4)). SU(4) group

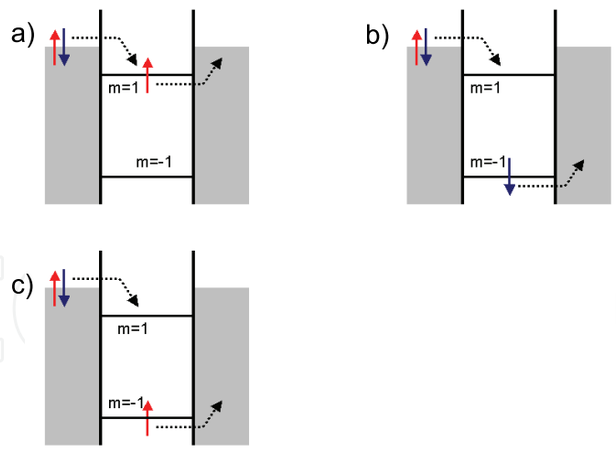


Fig. 5. Cotunneling processes leading to quenching of spin and orbital pseudospin in SU(4) quantum dot a) spin-flip fluctuation b) orbital fluctuation c) spin-orbital fluctuation.

characterizes the rotational invariance in spin and orbital space. The simultaneous screening of orbital and spin degrees is caused by tunneling processes causing spin, orbital pseudospin and spin-orbital fluctuations (Fig. 5). In this case orbital psudospins play exactly the same role as spins. The spectral density of SU(4) Kondo system shows a peak slightly shifted from the Fermi energy, it is pinned at $\omega \sim T_K^{SU(4)}$ (Fig. 6). The many-body peak is also

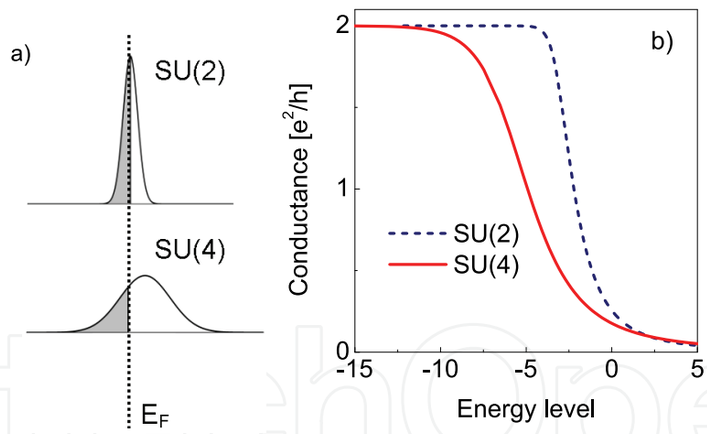


Fig. 6. Comparison of SU(4) and SU(2) Kondo effects a) Schematic view of Kondo resonances. SU(4) resonance is wider and shifted from the Fermi level. b) Conductance versus site energy.

much broader than that for the SU(2) Kondo effect, what means exponential enhancement of Kondo temperature. This makes these systems interesting for practical applications. Fig.6 shows a schematic picture of Kondo resonances for both symmetries and the corresponding dependencies of conductance on dot energy. The scattering phases at E_F are $\delta_{SU(2)} = \pi/2$ and $\delta_{SU(4)} = \pi/4$ respectively, and the zero temperature linear conductances $\mathcal{G}^{SU(2)} = 2(e^2/h)\sin^2(\delta_{SU(2)}) = \mathcal{G}^{SU(4)} = 4(e^2/h)\sin^2(\delta_{SU(4)}) = 2(e^2/h)$. Since in both cases total conductance reaches the same value one cannot reliably distinguish between SU(2) and SU(4) Kondo effect in the unitary limit based on the conductance analysis alone. It is worth to

mention that for higher degeneracies total conductances diminish, what is easy to check putting the values of phase shifts $\delta_{SU(2N)} = \pi/2N$. SU(4) Kondo effect in nanoscopic systems has been first observed for vertical QDs (Sasaki et al., 2004), but most spectacular evidence of this phenomena has been reported by Jarillo-Herrero et al. for carbon nanotubes (Jarillo-Herrero et al., 2005). Fig. 7 presents how formation of Kondo resonance manifests in the differential conductance. The conductance exhibits a pronounced enhancements in regions for 1 and 3 electrons. The estimated Kondo temperature for the discussed system was $T_K = 7.7$ K what can be ascribed to the enhanced degeneracy. A confirmation that the observed phenomena is really spin-orbital Kondo effect is the influence of finite magnetic field on the low-energy Kondo behavior of conductance. For perpendicular magnetic field, where only spin degeneracy is removed the splitting of high conductance line into three lines has been observed (Makarowski et al., 2007), for SU(2) symmetry only two lines should be visible. For the field applied parallel to the nanotube axis, when spin-orbital degeneracy is removed a splitting of the Kondo resonance into four peaks results (Fig. 7). A few

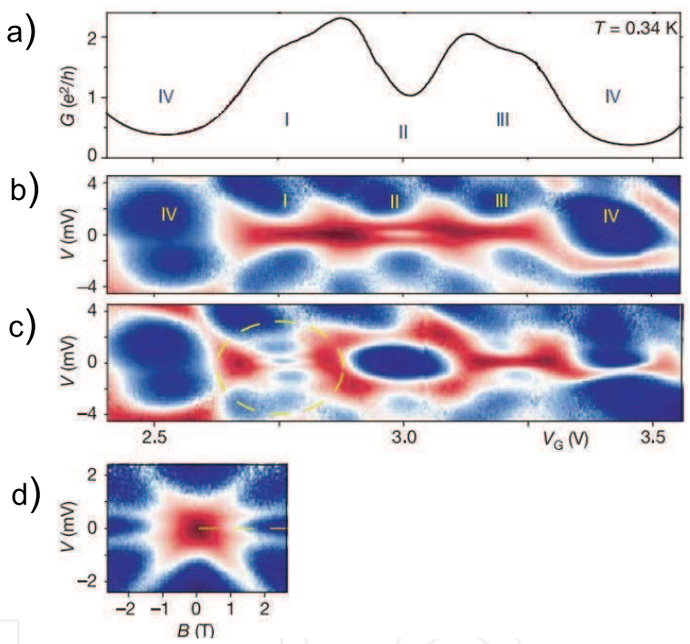


Fig. 7. Experimental evidence of SU(4) Kondo effect in semiconducting carbon nanotube quantum dot. a) Linear conductance versus gate voltage at 0.34 K. Latin numbers classify the valleys according to the occupations at the dot. b) Color-scale plot of differential conductance versus gate and transport voltages at zero magnetic field. Conductance increases from blue to red. The enhanced linear conductance signals the occurrence of Kondo effect. c) Same as b) but for CNT-QD in axial magnetic field $h_{||} = 1.5$ T. d) Fourfold splitting of the Kondo peak as a function of field. Adapted from ((Jarillo-Herrero et al., 2005)).

observations of spin-orbital Kondo effect in CNTs (Grove-Rasmussen et al., 2007; Wu et al., 2009) and several interesting theoretical papers on SU(4) Kondo problem have been published very recently (Büsser & Martins, 2007; Choi et al., 2005; Galpin et al., 2006; Lim et al., 2006; Lipiński & Krychowski, 2005; Mizumo et al., 2009). The unusual strongly correlated Fermi liquid state, where spin and orbital degrees of freedom are totally entangled is interesting for quantum computing and storage technology. Doubling of storage density is expected, because

each 4-state bit is exactly equivalent to two 2-state bits. The exotic spin-orbital Kondo effect occurs if the orbital quantum number is conserved during tunneling. If the leads to the dot are formed within the same nanotube this requirement is fulfilled, otherwise some mixing in the orbital channels may occur. It is surprising therefore that SU(4) Kondo effect is observed with metallic electrodes attached. Some authors suggest (Choi et al., 2005) that, in these systems, the orbital quantum number is still conserved during higher order tunneling events, probably because the CNT-QD is coupled to the nanotube section underneath the contacts, where the carriers dwell for some time before moving into the metal. Even for small mixing of orbital channels (mixing smaller than the Kondo energy) the SU(4) Kondo description can still serve as a reasonable first insight into physics of these systems.

4. Model and formalism

CNT-QD exhibits four-fold shell structure in the low energy spectrum. In the present considerations we restrict to the single shell, what is justified for short nanotubes at low temperatures, because the level spacing in this case is larger than thermal energy. We take into account only the top most occupied shell and treat other electrons as inert core. The dot is modeled by two-orbital Anderson impurity model:

$$\begin{aligned}\mathcal{H} &= \sum_{k\alpha m\sigma} \epsilon_{k\alpha m\sigma} c^{+}_{k\alpha m\sigma} c_{k\alpha m\sigma} + \sum_{k\alpha m\sigma} t_{\alpha}(c^{+}_{k\alpha m\sigma} d_{m\sigma} + h.c) \\ &+ \sum_{m\sigma} E_{m\sigma} d^{+}_{m\sigma} d_{m\sigma} + \sum_{m} \mathcal{U} n_{m+} n_{m-} + \sum_{\sigma\sigma'} \mathcal{U}' n_{1\sigma} n_{-1\sigma'} \end{aligned} \quad (1)$$

where $m = \pm 1$ numbers the orbitals, the leads channels are labeled by (m, α), $\alpha = L, R$. $E_{m\sigma} = E_0 + eV_g + g\mu_B h + g\mu_{orb} h\cos(\theta)$, we set $|e| = g = \mu_B = k_B = \hbar = 1$. θ specifies orientation of magnetic field h relative to the nanotube axis, μ_{orb} is the orbital moment. The first term of (1) describes electrons in the electrodes, the second describes tunneling to the leads, the third represents the dot site energy and the last two terms account for intra ($\mathcal{U}$) and interobrbital ($\mathcal{U}'$) Coulomb interactions. We will consider carbon nanotubes coupled to electrodes which can be either nonmagnetic or ferromagnetic. The spin polarization of the leads P_α is defined by spin-dependent densities of states $\varrho_{\alpha m\sigma}$ as $P_\alpha = (\varrho_{\alpha+} - \varrho_{\alpha-})/(\varrho_{\alpha+} + \varrho_{\alpha-})$. The spin-dependent coupling strength to the lead Γ is described by $\Gamma = \sum_\alpha \Gamma_\alpha = \sum_{km\alpha\sigma} \pi t^2_\alpha \varrho_{\alpha m\sigma}$. In the following, the wide conduction-band approximation with the rectangular density of states is used $\rho_{\alpha m\sigma}(\epsilon) = \rho_{\alpha\sigma} = 1/(2\mathcal{D}_{\alpha\sigma})$ for $|\epsilon| < \mathcal{D}_{\alpha\sigma}$, $\mathcal{D}_{\alpha\sigma}$ is the half bandwidth.

We are interested in nonequilibrium properties e.g. in current flowing through the dot. A common tool used in the description of transport characteristics are nonequilibrium Green's functions of Keldysh type, defined as a path-ordered product of annihilation and creation operators on a closed time contour which begins and ends at the same point. For a review of the techniques of the nonequilibrium Green's functions and its applications in electronic transport we refer the reader to (Haug & Jauho, 1998). In our discussion, instead of performing contour integration we adopt approximation known as Ng ansatz (Ng, 1996), which allows construct approximate nonequilibrium function for interacting system from the knowledge of equilibrium functions and nonequilibrium characteristics of the corresponding noninteracting system. The exact values of the latter can be easily found. Commonly used nonequilibrium Green's functions are lesser $G^{<}_{m\sigma,m\sigma}(t-t') = i\langle d^{+}_{m\sigma}(t') d_{m\sigma}(t)\rangle$ and greater $G^{>}_{m\sigma,m\sigma}(t-t') = -i\langle d_{m\sigma}(t) d^{+}_{m\sigma}(t')\rangle$ functions. They are linked with ordinary retarded or advanced Green's functions $G^{R}_{m\sigma,m\sigma}(t-t') = -i\theta(t-t')\langle[d_{m\sigma}(t), d^{+}_{m\sigma}(t')]\rangle$, $G^{A}_{m\sigma,m\sigma}(t-t') =$

$i\theta(t'-t)\langle[d_{m\sigma}(t), d^{+}_{m\sigma}(t')]\rangle$ through the relation $\mathbf{G}^{>} - \mathbf{G}^{<} = \mathbf{G}^{\mathbf{R}} - \mathbf{G}^{\mathbf{A}}$. Accordingly linked are also corresponding self energies $\mathbf{\Sigma}^{>} - \mathbf{\Sigma}^{<} = \mathbf{\Sigma}^{\mathbf{R}} - \mathbf{\Sigma}^{\mathbf{A}}$ (Keldysh requirement). Ng ansatz assumes linearity of lesser self-energy $\mathbf{\Sigma}^{<}$ and lesser self energy of the corresponding noninteracting system $\mathbf{\Sigma}^{<} = \mathbf{\Lambda}\mathbf{\Sigma}^{<(\mathbf{0})}$, where $\mathbf{\Sigma}^{<(\mathbf{0})} = \sum_{\alpha} 2if_{\alpha}(\omega)\mathbf{\Gamma}_{\alpha}$. Coefficient, or in general case matrix $\mathbf{\Lambda}$, can be found from Keldysh requirement. Ng approximation is exact for noninteracting particles, and it preserves continuity of current condition in the steady-state limit (Ng, 1996).

Now a few words about approximations used in treating the many-body problem. Kondo effect is a consequence of strong electron correlations present in the system. For a correct description of physics in this range crucial is a preservation of dot electron-conduction electron correlations. The retarded Green's functions used in our analysis are found from the equation of motion method (EOM). EOM consists of differentiating the Green's functions with respect to time which generates the hierarchy of equations with higher order GFs. In order to truncate the series of equations, we use at the third step of the chain of equations the self-consistent procedure proposed by Lacroix (Lacroix, 1998), which approximates the GFs involving two conduction-electron operators by:

$$\begin{aligned}\langle\langle c^{+}_{k\alpha m'\sigma'} d_{m'\sigma'} c_{k\alpha m\sigma} | d^{+}_{m\sigma}\rangle\rangle &\simeq \langle c^{+}_{k\alpha m'\sigma'} d_{m'\sigma'}\rangle\langle\langle c_{k\alpha m\sigma} | d^{+}_{m\sigma}\rangle\rangle \\ \langle\langle c^{+}_{k\alpha m'\sigma'} c_{k\alpha m'\sigma'} d_{m\sigma} | d^{+}_{m\sigma}\rangle\rangle &\simeq \langle c^{+}_{k\alpha m'\sigma'} c_{k\alpha m'\sigma'}\rangle\langle\langle d_{m\sigma} | d^{+}_{m\sigma}\rangle\rangle \end{aligned} \tag{2}$$

Knowing G^{R} and G^{A} one calculates self energies Σ^{R} , Σ^{A}. The advantage of EOM method in comparison to other many-body techniques e.g. slave boson formalism often used in the analysis of Kondo limit (Coleman, 1987), is that EOM works in the whole parameter space except only the close vicinity of Kondo fixed point and it accounts not only for spin or pseudospin fluctuation, but also for charge fluctuations. This is of importance in analysis of systems with finite charging energy.

Let us now give few formulas determining quantities we study. Current flowing through CNT-QD in the $(m\sigma)$ channel $\mathcal{I}_{m\sigma} = (\mathcal{I}_{Lm\sigma} - \mathcal{I}_{Rm\sigma})/2$ is calculated from the time evolution of the occupation numbers $\hat{N}_{\alpha} = \sum_{km\sigma} c^{+}_{k\alpha m\sigma} c_{k\alpha m\sigma}$:

$$\begin{aligned}\mathcal{I}_{\alpha}(t) = \; & -e\langle d\hat{N}_{\alpha}(t)/dt\rangle = i(e/\hbar)\sum_{km\sigma}[t_{\alpha}\langle c^{+}_{k\alpha m\sigma}(t) d_{m\sigma}(t)\rangle - h.c.] = \\ & = \sum_{km} t_{\alpha}[G^{<}_{m\sigma,k\alpha m\sigma}(t) - G^{<}_{k\alpha m\sigma,m\sigma}(t)] \end{aligned} \tag{3}$$

The thermal averages are expressed by the lesser Green's function as:

$$\langle c^{+}_{k\alpha m\sigma} d_{m\sigma}\rangle = \int \frac{d\omega}{2\pi i} G^{<}_{m\sigma,k\alpha m\sigma}(\omega) \tag{4}$$

Conductances are defined as $\mathcal{G}_{\sigma} = d\mathcal{I}_{\sigma}/dV = \sum_{m} d\mathcal{I}_{m\sigma}/dV$. The useful quantities characterizing the spin-dependent transport are polarization of conductance $\mathcal{PC} = (\mathcal{G}_{+} - \mathcal{G}_{-})/(\mathcal{G}_{+} + \mathcal{G}_{-})$ and tunnel magnetoresitance ($\mathcal{TMR}$). Tunnel magnetoresistance is defined as the relative difference of differential conductances for parallel (P) and antiparallel (AP) configurations of polarizations of the leads $\mathcal{TMR} = (\mathcal{G}^{\mathcal{P}} - \mathcal{G}^{\mathcal{AP}})/\mathcal{G}^{\mathcal{AP}}$. The spin transport is characterized by spin current. In general case apart from longitudinal component $\mathcal{I}^{z}$, which is easily expressible by the difference of charge currents for opposite spin channels $\mathcal{I}^{z} = \mathcal{I}_{+} - \mathcal{I}_{-}$, also transverse (spin flip currents) are required. $\mathcal{I}^{x} = Re[\mathcal{I}^{+}]$ and $\mathcal{I}^{y} = Im[\mathcal{I}^{+}]$. $\mathcal{I}^{+} = (\mathcal{I}^{+}_{L} - \mathcal{I}^{+}_{R})/2$ can be expressed similarly as Eq.(3) by $\mathcal{I}^{+}_{\alpha}(t) =$

$2\sum_{km} t_\alpha [G^<_{m-,k\alpha m+}(t) - G^<_{k\alpha m-,m+}(t)]$. To supplement transport characteristics we will also present discussion of the shot noise. The shot noise reveals information of transport which are not accessible by knowledge of conductance alone, for example about the correlations. The temporal fluctuations of the current are defined as:

$$\mathcal{S}_{\alpha m\sigma\nu m'\sigma'}(t-t') = \langle [\Delta\hat{\mathcal{I}}_{\alpha m\sigma}(t), \Delta\hat{\mathcal{I}}_{\nu m'\sigma'}(t')]_+ \rangle = \langle [\hat{\mathcal{I}}_{\alpha m\sigma}(t), \hat{\mathcal{I}}_{\nu m'\sigma'}(t')]_+ \rangle - 2\cdot \mathcal{I}_{\alpha m\sigma}(t)\mathcal{I}_{\nu m'\sigma'}(t') \quad (5)$$

where $\Delta\hat{\mathcal{I}}_{\alpha m\sigma}(t)$ is the fluctuation of the current operator around its average value. At very small bias ($eV < k_BT$) noise is dominated by thermal noise. The thermal noise is related to fluctuations in the occupations of the leads due to thermal excitation, and vanishes at zero temperature. Contribution to the noise, we are interested in - shot noise is an unavoidable temporal fluctuation of current caused by the discreteness of the electronic charge (Blanter & Büttiker, 2000). Current is not a continuous flow, but a sum of discrete pulses in time, each corresponding to the transfer of an electron through the system. If the electrons are transmitted randomly, independently of each other the transfer of them can be described by Poissonian statistics. Deviations from the Poissonian noise appear to be due to correlations between electrons. A convenient means to assess how correlations affect shot noise is the Fano factor $\mathcal{F}$ defined as the ratio between the actual shot noise $\mathcal{S}$ and the Poissonian noise $\mathcal{F} = \mathcal{S}/(2e\mathcal{I})$.

Let us close this section by a few words on the energy scale of the effects examined. In the full symmetric case SU(4) (equal coupling to the leads and equal inter and intraorbital interactions) the behavior of the model is governed by four parameters, two of them specify the dot: orbital energy E_0 and single electron charging energy $\mathcal{U}$. Another two parameters characterize the coupling to the leads - Γ, and the leads themselves - the half bandwidth $\mathcal{D}$. Tunnel barrier widths and source and drain capacitances change with the number of electrons at the dot and consequently both lead - dot coupling and charging energy change with the gate voltage. By gate voltage one can directly control the site energy. The value of $\mathcal{U}$ can be inferred from the size of Coulomb diamonds, for semiconducting CNT-QDs it takes values of order of tens meV (Babić et al., 2004; Jarillo-Herrero et al., 2004). Intermediate coupling strength required in the Kondo range corresponds to Γ of order of several meV (Jarillo-Herrero et al., 2005; Makarowski et al., 2007). $\mathcal{D}$ is the largest energy scale in our problem and it is of order of tens of meV. Choosing parameters of CNT-QD within the above intervals of parameters gives estimation of Kondo temperature in the range of several Kelvin, what agrees with characteristic temperatures observed in these systems. Typical diameter d of SWNCT is of order of several nm. Orbital magnetic moment μ_{orb} scales with CNT diameter and can be estimated from the slopes between two Coulomb peaks that correspond to the addition energy of the electrons to the same orbital. We assume $\mu_{orb} = 10\mu_B$, which corresponds to the diameter $d = 2.9$ nm. In the following pictures, all the energies are given in units of Γ and similarly other quantities in accordance with the earlier chosen sets of the units ($|e| = q = \mu_B = k_B = \hbar = 1$). The bandwidth $\mathcal{D}$ is assumed $\mathcal{D} = 50$.

5. SU(4) Kondo effect in carbon nanotube quantum dot

Until recently, the prospect of using the Kondo effect in spintronic applications have been very poor because the required temperatures for semiconducting QDs lie in mK range. The use of single wall carbon nanotubes as quantum dots has pushed the Kondo temperatures to the range of several K. In experiment of Jarillo-Herrero et al. (JH) the reported Kondo

temperature was $T_K \sim 7.7$ K (Jarillo-Herrero et al., 2005) and in (Makarowski et al., 2007) Kondo temperature as high as $T_K \sim 15$ K has been reported. Other properties which make CNT-QDs ideal candidates for electronic applications are long spin lifetimes and the fact that Kondo effect can be seen over a very wide range of gate voltages encompassing hundreds of Coulomb oscillations (Nygård et al., 2000). SU(4) Kondo effect in carbon nanotube is an example of many-body effect occurring for entangled degrees of freedom. In case of CNTs spin degrees of freedom are entangled with both chiralities of the nanotube. The SU(4) group is the minimal group allowing such spin-orbital entanglement and which guarantees rotational invariance both in spin and orbital spaces. In this section we investigate the SU(4) Kondo

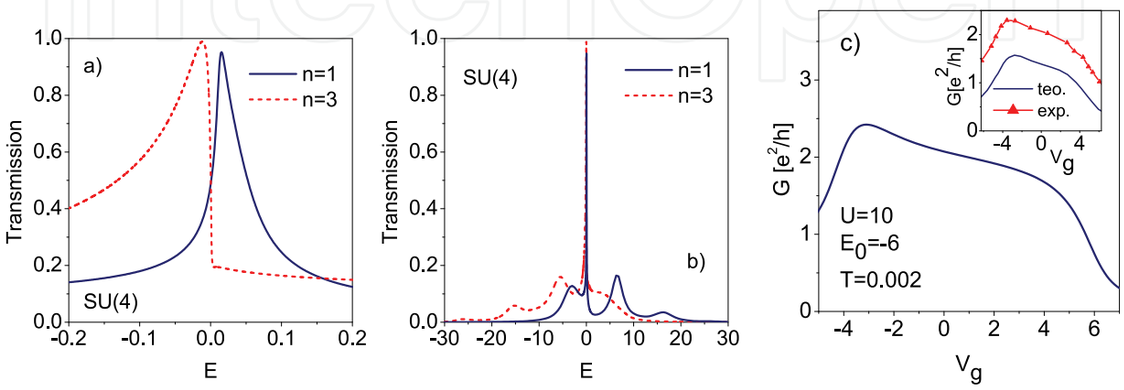


Fig. 8. a) Comparison of Kondo transmissions of CNT-QD in the range of single $n = 1$ and triple $n = 3$ electron occupations of the dot ($E_0 = -6, \mathcal{U} = 10$). b) Same as a) but shown in extended scale. The high energy peaks correspond to charge fluctuations. c) Gate dependence of linear conductance in the $n = 1$ range. Inset shows a similar dependence for CNT-QD parametrized by $E_0 = -6.25, \mathcal{U} = 12.5$ compared to the experimental curve ((Jarillo-Herrero et al., 2005)).

effect in the one and three electron valleys. For $n = 1$ both the total spin $S^z = (n_+ - n_-)/2$ and orbital pseudospin $T^z = (n_1 - n_{-1})/2$ are quenched due to spin-orbital fluctuations. For $n = 3$ the concepts of total spin or pseudospin is easier to understand replacing the electron occupations in definition of S^z or T^z by hole occupations. At very low temperatures the simple tunneling picture breaks down, scattering processes of any order contribute to the transport. The result is many-body state, which couples to the electrodes with a very high transmission probability, which as it is seen from Fig. 8 approaches one. The spin orbital fluctuations are also influenced by charge fluctuations. For infinite $\mathcal{U}$ the only charge fluctuations are ($n = 0 \leftrightarrow n = 1$), but for finite $\mathcal{U}$, which is the case considered, additional fluctuations ($n = 1 \leftrightarrow n = 2$) come into play. The role of these fluctuations for may-body processes is the larger the closer the corresponding charge fluctuation peaks are to the Fermi energy. Apart form the Coulomb peak ($\omega = E_0 + \mathcal{U}$) corresponding to fluctuation into the doubly occupied state, also a track of fluctuations into higher occupancy is visible. For $n = 1$ the Kondo peak occurs slightly above the Fermi level and dot occupation for the single spin-orbital channel is $n_{ms} \sim \frac{1}{4}$. The shift of the Kondo peak away from the Fermi level can be understood from Friedel sum rule (Langreth, 1966), which neglecting charge fluctuation perturbation, gives in this case scattering phase shift at E_F $\delta \sim \pi/4$. Accordingly, the linear conductance at zero temperature $\mathcal{G}(0) = 4(e^2/h)\sin^2(\delta) = 2(e^2/h)$. Charge fluctuations slightly modify this picture, but as it is seen conductance (transmission) is still close to the unitary limit. For $n = 3$ much broader Kondo resonance is formed below the Fermi level and electron occupation per

spin-orbital channel accounts $n_{ms} \sim 3/4$ (phase shift $\delta \sim (\frac{3}{4})\pi$). Charge fluctuations in both cases play different roles, what reflects in considerably different widths of Kondo resonances. Figure 8c shows the calculated gate dependence of linear conductance in the single dot occupancy. Values close to the unitary limit are observed for deep dot levels and a drop of the conductance is visible when gate voltage moves the system closer to the mixed valence range. We also show in the inset a similar gate dependence of conductance calculated for another choice of parameters, which nicely reproduces the shape of experimental gate dependences reported in (Jarillo-Herrero et al., 2005) (compare conductance in region I on Fig. 7a). This fitting to experiment has been reported by us earlier in (Krychowski & Lipiński, 2009). As it is seen the calculated conductance is underestimated in comparison to experimental value by a constant value of $0.5(e^2/h)$ in the whole gate range. This background contribution can be ascribed to possibly additional non-Kondo conductance channel present in the system and neglected in our analysis.

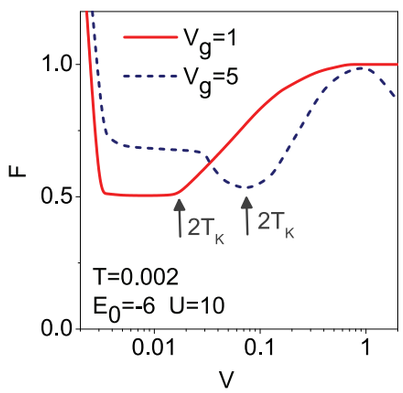


Fig. 9. Bias dependence of shot noise Fano factor. Low bias noise suppression induced by Kondo correlations is not complete ($\mathcal{F} = 1/2$).

Summarizing, in fully symmetric SU(4) state the four states at the dot are degenerate. Quantum fluctuations between these states induced by coupling to the leads (coupled fluctuations in spin and orbital sectors) result in formation of highly correlated Fermi liquid state, where spin and orbital degrees of freedom are totally entangled. Kondo resonance is no longer peaked at E_F and Kondo temperature is largely enhanced in comparison to SU(2) systems. The linear conductance cannot reliably distinguish between SU(2) and SU(4) Kondo effects in the unitary limits (see Figure 6). As we will discuss in the next section, the field evolution of conductance is different for two cases, and this allows identify the type of Kondo effect. Distinction between two cases can be done also analyzing the shot noise. For SU(2) symmetry, the shot noise vanishes ($\mathcal{F} = 0$). Results presented on Fig. 9 display that due to the entanglement the SU(4) system remains noisy in the Kondo range, the Fano factor does not vanish. This fact has been recently observed in CNT-QDs (Delattre et al., 2009). For $V \sim 2T_K$ Fano factor takes the value $\mathcal{F} = \frac{1}{2}$ for the deep dot level position ($V_g = 1$) or slightly higher in the range closer to mixed valence ($V_g = 5$). In the latter case also the limit of constant value of $\mathcal{F}$ is not preserved in the whole low bias range due to a shallow dip in the Kondo peak introduced by charge fluctuations. At extremely small bias a rapid increase of $\mathcal{F}$ is observed and it is due to the fact that noise is dominated by thermal noise in this case. Fano factor is $(2T)/V$ in this range due to fluctuation-dissipation theorem and divergent at $V = 0$. For high voltages $V > 2T_K$ an increase of $\mathcal{F}$ is visible due to the weakening of Kondo correlations.

Maximum of $\mathcal{F}(V)$ for curve corresponding to $V_g = 5$ and the following decrease of $\mathcal{F}$ is due to Coulomb charge fluctuations. For the deep dot level the influence of these fluctuations is less significant and a drop of bias dependence of Fano factor is observed for still higher voltages beyond the presented range.

6. Effect of magnetic field

In the following sections we will discuss impact of symmetry-breaking perturbations on transport through CNT-QD in the Kondo regime. Since our study is addressed to spintronics we will analyze the effect of magnetic field and polarizations of electrodes. Field perpendicular to the nanotube axis breaks only the spin degeneracy and parallel field breaks both spin and orbital degeneracy. When an axial magnetic field is applied to CNTs, the electronic states are modified by an Aharonov-Bohm phase (A-B). The A-B phase affects electron states differently depending on the orbital quantum number. Quantization condition for momentum in the circumferential direction is now generalized to:

$$\pi d \cdot k_{\perp} + (2\pi)\frac{\varphi}{\varphi_0} = (2\pi)i \quad (i = 1, 2..., \ h_{||} \neq 0), \tag{6}$$

where $(2\pi)\frac{\varphi}{\varphi_0}$ is A-B phase acquired by the electrons while traveling the nantube circumference ($\varphi = h_{||}\pi d^2/4$ and φ_0 is the flux quantum). The splitting of the states numbered by opposite orbital numbers can be expressed similar to Zeeman splitting in terms of orbital magnetic moment by the term $m\mu_{orb}$ included in definition of Hamiltonian (1), $\mu_{orb} = (e|v_F|d)/4$. Orbital moment scales with CNT diameter and is typically one order of magnitude larger than Bohr magneton. This fact is the reason for strong magnetic field anisotropy of conductance of CNT-QD, the orbital pseudospin is more susceptible to magnetic field than the real spin. Already at small axial fields a considerable change of conductance is observed. For the shallow site energy, when unperturbed Kondo peak is noticeably shifted from Fermi level the field induced emergence of orbital satellites on both sides of the main peak and a shift of one of them towards the Fermi level (Fig. 10c) results in the observed initial increase of the linear conductance. Further increase of the field reflects in the decrease of conductance, and it happens when the lower satellite moves below E_F. For high magnetic field also spin splitting is visible (Fig. 10d). For perpendicular orientations the orbital motion is unaffected by the field, and only spin splitting results in high magnetic fields, for small fields only a slight shift of the peak towards Fermi level and its broadening leading to the increase of DOS at E_F, what leads to the corresponding increase of conductance. For deeper site energies the similar reconstructions of the Kondo peak in the field results in the decrease of conductance in both cases (Fig. 10b), because the unperturbed resonance is closely located to E_F. Figs. 10e, f present finite bias and magnetic field differential conductance maps. For axial field four lines and for perpendicular three lines of high conductance are visible. A pair of inner lines on Fig. 10e corresponds to orbital conserving fluctuations for both spin channels and the outer lines reflect orbital and simultaneous spin and orbital fluctuations. The latter two processes are not resolved for the assumed value of coupling to the leads and temperature. This picture qualitatively reflects the field dependence observed in (Jarillo-Herrero et al., 2005) (compare Fig. 7c, d). The difference between the $n = 1$ and $n = 3$ behaviors in the parallel field has been reported in (Jarillo-Herrero et al., 2005; Makarowski et al., 2007). For the first region the four line structure has been observed whereas for the second region only three lines were visible. This fact has been interpreted in (Galpin et al., 2010) as a consequence of spin-orbit interaction,

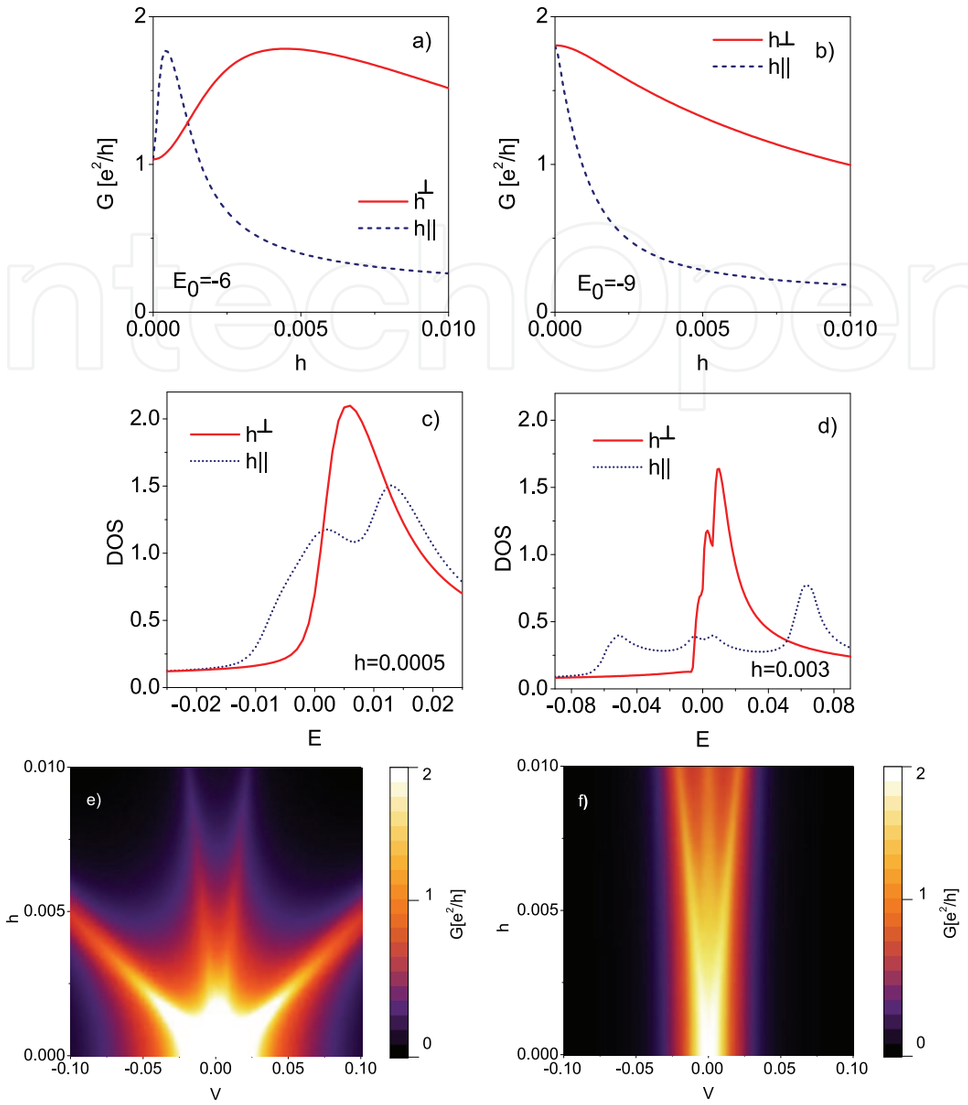


Fig. 10. Magnetic field anisotropy of conductance of CNT-QD in the Kondo regime. a) Magnetic field dependence of conductance for parallel and perpendicular orientations for the dot energy $E_0 = -6$ ($\mathcal{U} = 15$). b) Same as a) but for the deeper dot energy $E_0 = -9$. c) DOS of CNT-QD ($E_0 = -6$) for small magnetic field. d) Same as c) for high magnetic field e) Color-scale plots of differential conductance versus axial field and bias voltage ($E_0 = -9$). f) Same as e) but for perpendicular field.

but alternatively one can think that it is only a consequence of difference of the widths of unperturbed Kondo peaks resulting from different roles played by charge fluctuations in both cases (compare e.g. Fig. 8a). For $n = 3$ at moderate fields the lines corresponding to different spin orientations are not resolved from the main peak. A careful look at the JH conductance maps also supports this point of view, since also in their pictures only three lines are visible for low values of axial field. Typically three lines structure occurs for the perpendicular field orientation. The central line corresponds to the orbital fluctuations and the outer lines are due to spin mixing fluctuations. The experimental confirmation of such behavior can be

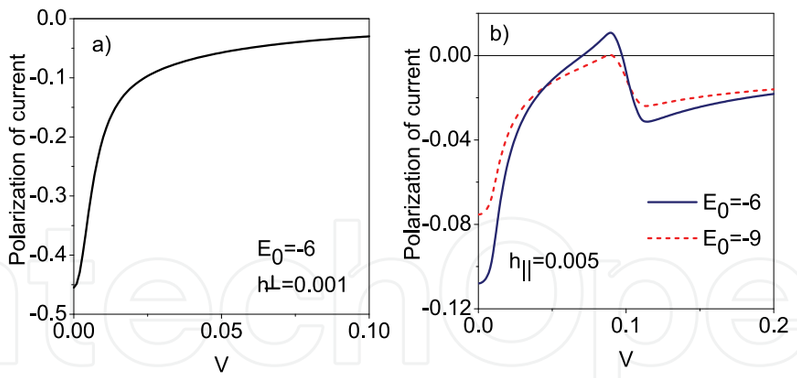


Fig. 11. Bias dependences of polarization of currents in a) perpendicular b) parallel magnetic fields.

found in (Makarowski et al., 2007). More detailed comparison to experiment including the relevant parameters and considering the asymmetry of the leads has been published by us in (Krychowski & Lipiński, 2009).
Current flowing in magnetic field is spin polarized. Fig. 11 presents an example of polarization of current $(\mathcal{I}_+ - \mathcal{I}_-)/(\mathcal{I}_+ + \mathcal{I}_-)$ corresponding to colorscale plot of differential conductance presented at Fig. 10. Substantial polarization of current is observed for small bias. Polarization can change its sign when spin-orbital Kondo satellites enter transport window. For high voltages ($eV \gg g\mu_B h$) current becomes unpolarized.

7. Kondo spin filter

Spin filter is a device that filters electrons by their spin orientation. Controlling the spin degree of freedom is currently an important challenge in spintronics. In particular in quantum information technology spin filters can be used for initialization and readout of spin quantum bits (Loss & DiVincenzo, 1998). Recently we have shown (Krychowski et al., 2007), that

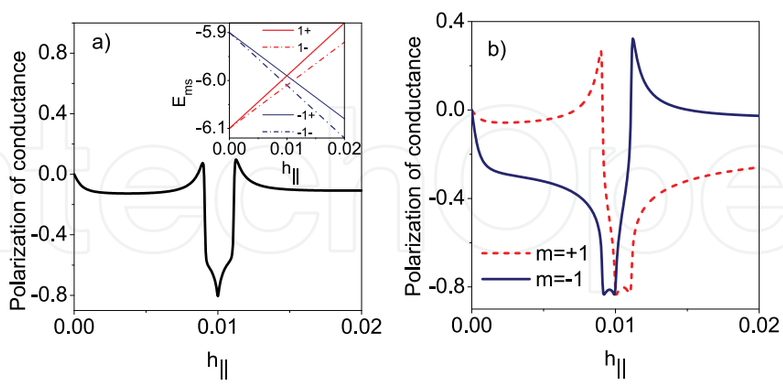


Fig. 12. Spin polarization of conductance of CNT-QD characterized by orbital level mismatch $\Delta_{orb} = 0.1$ in axial magnetic field. Inset illustrates recovery of orbital degeneracy. b) Orbital resolved spin polarizations corresponding to the picture a).

CNT-QD characterized by orbital level mismatch $\Delta_{orb} = E_{1\sigma} - E_{-1\sigma} \neq 0$ can serve as efficient spin filter operating in the low field range. Orbital mismatch occurs e.g. in nanotubes with torsional deformation. Fig. 12 presents polarization of total conductance and orbital resolved

polarizations versus axial magnetic field. The idea of the proposed spin filtering mechanism is explained in the inset of Fig. 12a. Magnetic field is exploited to tune spin-polarized states into orbital dengeracy. Axial field might recover the orbital degeneracy either within the same spin sector or with mixing of spin channels. In the former case ($h_{||} = \Delta_{orb}/(2\mu_{orb})$) almost the same polarizations of conductance are observed for both orbital channels what results in large total polarization, whereas for the latter case ($h_{||} = \Delta_{orb}/(2\mu_{orb} + 1)$) the spin polarizations of different orbital sectors have opposite signs. Taking $\Delta_{orb} = 0.1$ meV gives estimation for the required fields for filtering 86 mT.

8. Kondo spin valve

The simplest two-terminal spintronic device is spin valve, on which the read heads of hard drives and MRAMs are based. Fig. 13 presents spin valve in which carbon nanotube is attached to two ferromagnetic electrodes. The technology of coupling CNTs to ferromagnetic electrodes e.g. to Co, Fe, Ni , NiPd leads is well elaborated (Cottet et al., 2006) and interesting experimental results have been published, also in the Kondo range (Hauptmann at al., 2008). These data concern however SU(2) symmetry in metallic carbon nanotubes contacted to ferromagnetic leads. There is also rich theoretical literature on Kondo effect in quantum dot coupled to magnetic leads, but with exception of our recent paper (Lipiński & Krychowski, 2010) all of them also apply only to SU(2) symmetry (e.g. (Bułka & Lipiński, 2003; Choi et al., 2004; Martinek et al., 2003; Sergueev et al., 2002; Świrkowicz et al., 2006)). In the following we discuss SU(4) case. To control the transport the dependence on the relative orientation of magnetic moments of the leads is exploited. Polarization of electrodes breaks the spin

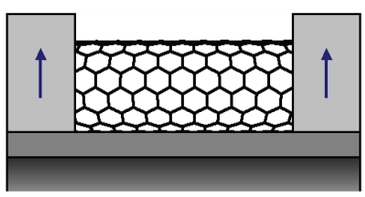


Fig. 13. Schematic view of spin valve. CNT-QD contacted to ferromagnetic electrodes, polarizations of which might be oriented either parallel or antiparallel.

degeneracy. Different tunneling rates for up and down spin electrons result in different widths of Kondo peaks for each spin channel. There is however also more crucial impact of polarization on Kondo resonance, which manifests most strongly close to the charge degeneracy points. Charge fluctuations are spin-dependent and they induce an effective exchange field. To find the spin splitting we use, following (Martinek et al., 2005) the Haldane scaling approach (Haldane, 1978), where charge fluctuations are integrated out, but effectively introduce spin dependent renormalization of the effective dot energies. We do not write here the resulting analytic form of exchange splitting ($\Delta_{exch.} = E_{m+} - E_{m-}$) , which can be found e.g. in (Martinek et al., 2005), but only present on Fig. 14f an example of its gate dependence. We see that not only the magnitude of this splitting, but also the sign changes with gate voltage. Controlling the spin degree of freedom by purely electrical means is currently an important challenge of spintronics. In contrast to an applied magnetic field, it acts rapidly and allows very localized addressing. To control the transport in spin valves the dependence on the relative orientation of magnetic moments of the leads is exploited. Figs. 14a, b present bias dependencies of $\mathcal{TMR}$ for negative and positive exchange fields. Linear $\mathcal{TMR}$ reaches for

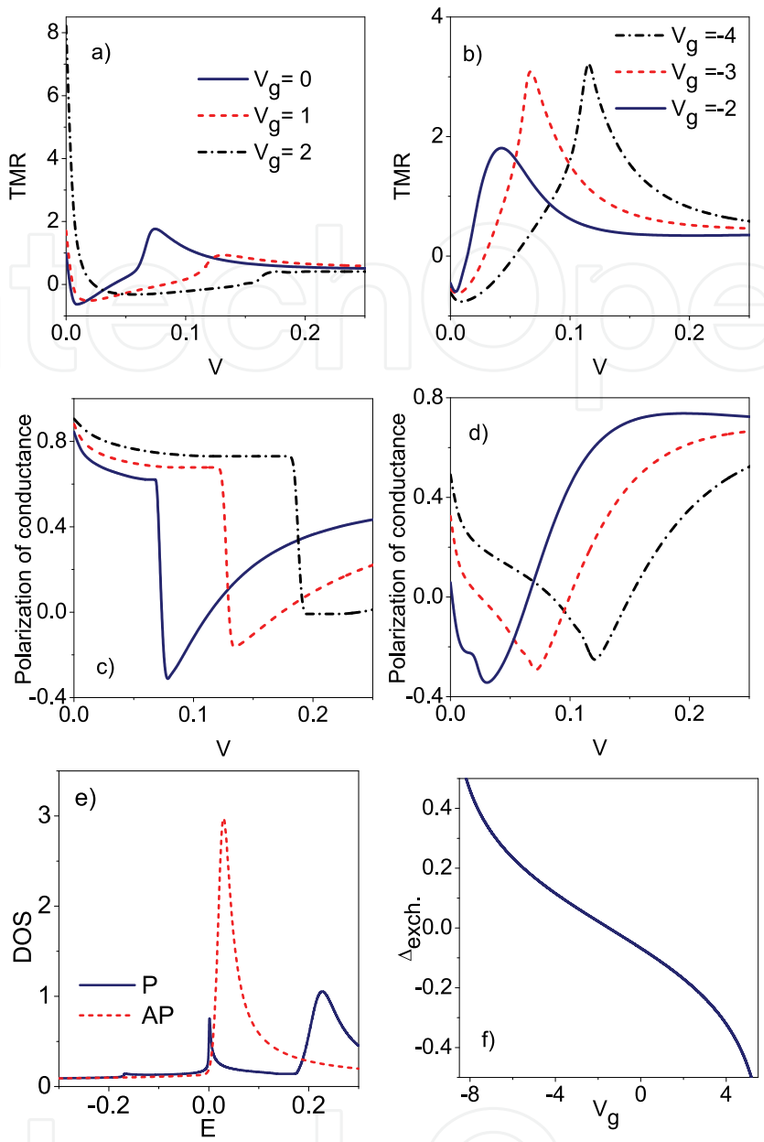


Fig. 14. Bias dependencies of tunnel magnetoresistance for negative (a) and positive (b) exchange splitting. Compare Fig. 14f. c,d) Polarizations of conductance for parallel configuration. Marking of the curves corresponds to the same gate assignment as on Figs a, b) e) Density of states of CNT-QD for parallel and antiparallel configurations f) Gate dependence of exchange splitting for $P = 0.6$, dot parameters are $E_0 = -6, \mathcal{U} = 15$.

$V_g = 2$ ($\Delta_{exch.} = -0.2$) giant value of 800%. Positive value of linear $\mathcal{TMR}$ means dominance of DOS at the Fermi level for parallel orientation of polarizations of electrodes $\varrho_P(E_F)$ relative to DOS for antiparallel configuration $\varrho_{AP}(E_F)$. This is the case presented e.g. on Fig. 14e. In the opposite case ($\Delta_{exch.} > 0$) AP density of states (or transmission) dominates over P transmission what results in negative (inverse $\mathcal{TMR}$). Important message following from the above observation is that one can control $\mathcal{TMR}$ electrically by the change of gate voltage. The sharpness of the peak of DOS for P configuration is the reason of the observed dramatic change of $\mathcal{TMR}$ in the low voltage range leading even to a change of sign (Fig. 14a). For

P configuration the three peak structure is visible for sufficiently high exchange field. The satellites are resolved from the main peak if $|\Delta_{exch.}| > T_K$. The central peak corresponds to orbital fluctuations and the side peaks to spin and spin-orbital fluctuations. For parallel orientation differential conductance sharply increases close to bias voltage equal to exchange splitting $V \sim \Delta_{exch.}$ and it reflects in the occurrence of peaks of $\mathcal{TMR}$. For high voltages magnetoresistance saturates and reaches value close to Juliére limit for uncorrelated electrons (Julliére, 1975). A small difference is a consequence of the influence of charge fluctuations occurring for higher energies (Juliére limit for $P = 0.6$ is $P^2(1 - P^2) = 0.56$). Figures 14c, d present bias dependencies of polarizations of conductance for parallel configuration. Minima of PC coincide with maxima of $\mathcal{TMR}$ and occur for voltages equal to exchange splitting. Due to the asymmetric shape of Kondo satellites (Fig. 14e) and reverse of positions of up and down peaks with the change of the sign of exchange field, modification of character of bias dependence of PC is observed. For positive exchange splitting a gradual change of

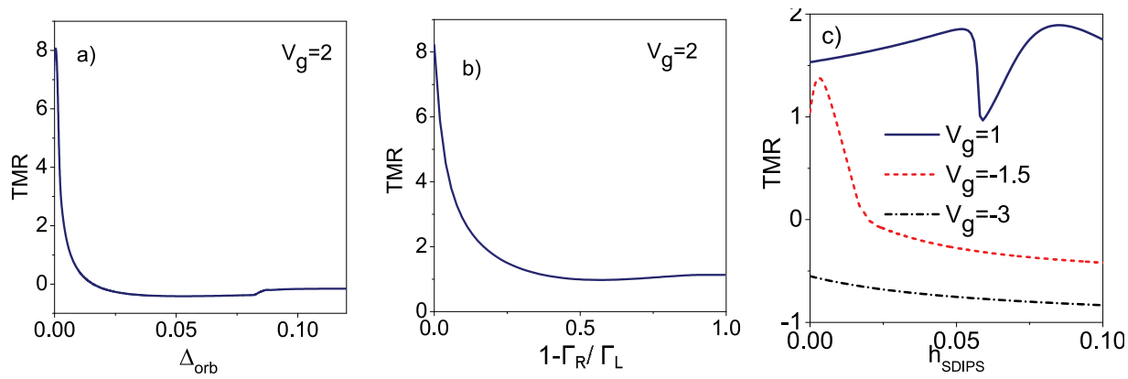


Fig. 15. a) TMR dependence on the orbital level mismatch Δ_{orb} ($V_g = 2$). b) TMR dependence on asymmetry of coupling $1 - \Gamma_R/\Gamma_R$ ($V_g = 2$). c) Influence of interfacial spin scattering on magnetoresistance of CNT-QD ($P = 0.6$, $E_0 = -6, \mathcal{U} = 15$).

PC is seen near $V \sim \Delta_{exch.}$ whereas for negative a sharp jump occurs. The corresponding bias dependence of polarization of current, not presented here, would resemble the one discussed earlier for magnetic field (Fig. 11). The question arises how robust is $\mathcal{TMR}$ against geometrical disturbances, since the full symmetric case is not easily accessible in experiment due to residual symmetry breaking perturbations. Two examples of influence of nonmagnetic perturbations on $\mathcal{TMR}$ are shown on Fig. 15 - the effect of level mismatch and impact of asymmetry in the coupling. It is seen that in order to record giant $\mathcal{TMR}$ values ideal nanotubes symmetrically coupled to the leads are desired. Before concluding this section, let us make a remark on another possible contribution to the spin splitting of the conductance peaks. The interface between a ferromagnet and quantum dot can scatter electrons with spin parallel or antiparallel to the magnetization of the lead with different phase shifts. This spin dependence of interfacial phase shift (SDIPS) can significantly modify spin dependent transport in the peculiarity $\mathcal{TMR}$. Phenomenologically one can introduce the effect of SDIPS as Zeeman splitting induced by an effective field h_{SDIPS} (Cottet & Choi, 2006). This can be justified physically on the following ground. For a double barrier system, the ferromagnetic exchange field makes the confinement potential of electrons on the dot spin dependent. This naturally induces a spin dependence of orbital energies (Cottet et al., 2006). Orbital energy $E_{m\sigma}$ Eq. (1) should be supplemented therefore by the term $g\sigma\mu_B h_{SDIPS}$. The introduced effective field depends on the configuration of electrodes and it vanishes for AP configuration

with symmetrical coupling. The effect of interfacial spin scattering on $\mathcal{TMR}$ have been discussed by us in (Krychowski & Lipiński, 2008) for the case of vanishing exchange splitting. Here we present the example of calculated magnetoresistance when both exchange splitting and h_{SDIPS} have been taken into account (Fig. 15c). It is seen, that spin activity of the interface can considerably modify $\mathcal{TMR}$ and even change its sign. For gate voltage $V_g = 1$ exchange field is negative and thus acts contrary to the positive spin scattering field what leads to the minimum of $\mathcal{TMR}$ when the two fields compensate. For vanishing exchange splitting ($V_g = -1.5$) in the range of small spin scattering fields $\mathcal{TMR}$ is determined by the difference of transmission rates for opposite spin channels, for higher values of h_{SDIPS}, $\mathcal{TMR}$ is determined almost entirely by this field and slightly decreases. Curve corresponding to $V_g = -3$ is an example where the action of one of the fields is amplified by another field and it results in strengthening of inverse $\mathcal{TMR}$. In the simple discussion presented above it was assumed that spin scattering field is gate independent. In general case both exchange and interfacial spin scattering fields are tunable with the gate voltage and the angle between ferromagnetic polarizations and this property could be exploited for manipulating spins and current flowing through the dot.

9. Spin currents

We extend our analysis by considering the spin-flip processes in the dot which mix the spin channels. They are represented by a perturbation:

$$\mathcal{H}' = \sum_m \mathcal{R}(d^+_{m+} d_{m-} + h.c) \tag{7}$$

Spin flips may be caused e.g., by transverse component of a local magnetic field. These processes are assumed to be coherent, in the sense that spin-flip strength $\mathcal{R}$ involves reversible transitions. Before discussion of spin currents let us first refer to the influence of spin flip processes on magnetoresistance, which is similar to the earlier mentioned effect of interfacial scattering field. The effect of spin flip transitions is illustrated on Fig. 16. Spin-flip makes

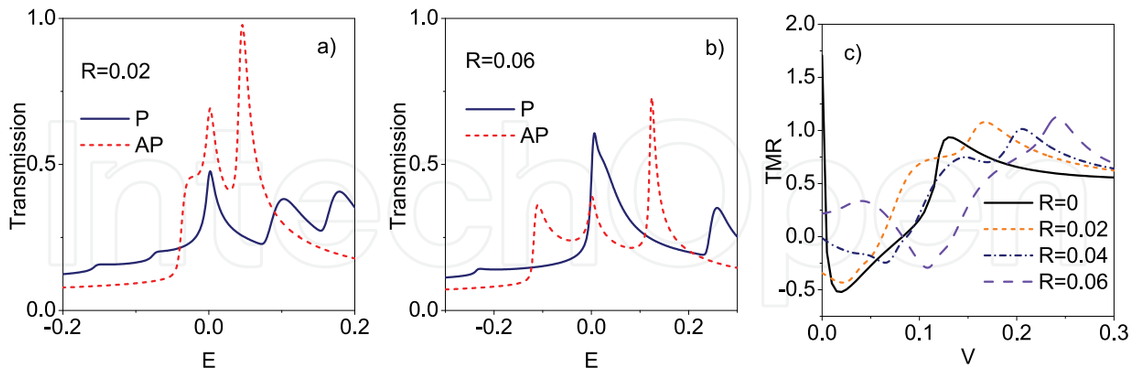


Fig. 16. Impact of spin-flip processes on $\mathcal{TMR}$. a) Transmissions for both spin polarization configurations for the weak spin flip scattering b) Same as a), but for strong spin-flip scattering. c) $\mathcal{TMR}$ for different values of spin-flip amplitude ($P = 0.6$, $E_0 = -5, \mathcal{U} = 15$).

the alignment of the lead polarizations less important. The resulting equilibration of the spin population leads to weakened magnetoresistance effect. The detailed behavior of $\mathcal{TMR}$ depends on the relative size of exchange splitting and spin flip transition amplitude. For the specific case shown on Fig. 16 linear $\mathcal{TMR}$ first rapidly decreases and changes sign with the

increase of $\mathcal{R}$ and then again becomes positive for larger $\mathcal{R}$. This can be understood looking at the plot of the evolution of the corresponding transmissions for parallel and antiparallel configurations (Figs 16a, b). For AP configuration for strong enough spin-flip amplitude the three peak structure is visible with satellites located roughly at $\omega \approx T_K \pm 2\mathcal{R}$. For P configurations the structure is richer, in the case of both large exchange splitting and strong spin-flip scattering the enhanced transmission is expected for $\omega \approx T_K \pm \Delta_{exch.} \pm 2\mathcal{R}$, but whether the separate peaks are well resolved or not depends on the relative strength of these two perturbations and Kondo energy. For $\mathcal{R} = 0.02$ AP transmission at E_F dominates over the P transmission and negative value of linear $\mathcal{TMR}$ is observed. For $\mathcal{R} = 0.06$ the opposite situation occurs and positive $\mathcal{TMR}$ is seen. The oscillating character of bias dependence of $\mathcal{TMR}$ reflects entering of the succeeding transmission peaks into the transport window. Whether the satellites mark on $\mathcal{TMR}$ curve as a distinct maximum or minimum or only as an inflection point, or are not visible at all, depends on the height of transmission peaks and their mutual separation on the energy scale. So far we have discussed a flow of spin polarized

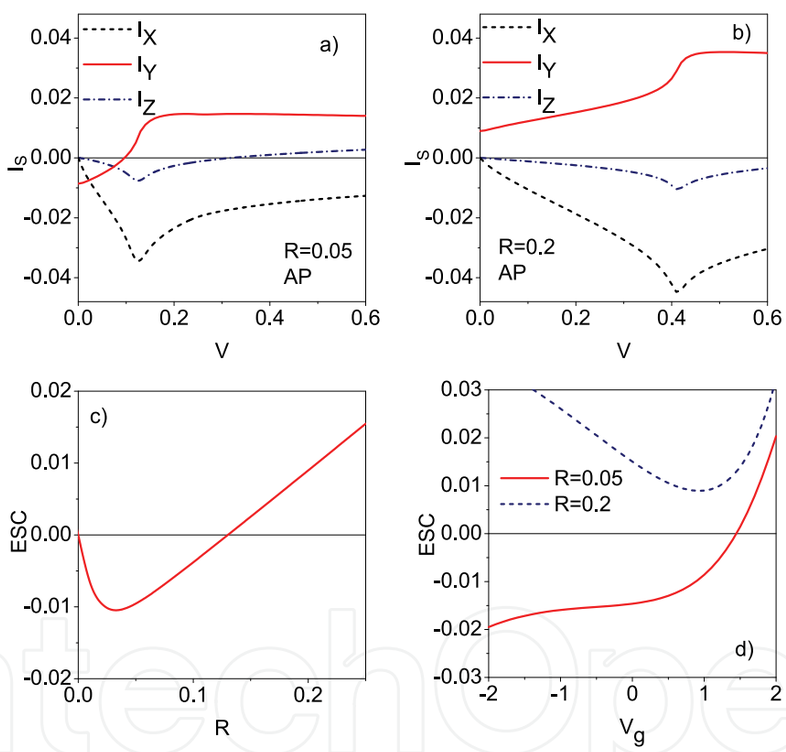


Fig. 17. a,b) Spin currents flowing through CNT-QD in the presence of spin-flip scattering for antiparallel configuration of polarizations of the leads. c) Dependence of equilibrium spin current $\mathcal{I}^y$ on spin-flip scattrering amplitude for AP configuration. d) Gate dependence of equilibrium spin current $\mathcal{I}^y$ for AP configuration ($P = 0.6$, $E_0 = -5, \mathcal{U} = 15$).

current through carbon nanotube quantum dot induced by presence of magnetic field or polarization of electrodes. More recently, there has been an increasing interest in generation of pure spin current without an accompanying charge current. Spintronic devices such as transistors (Žutić et al., 2004) require spin currents, just as conventional electronic devices require charge currents. The attractive attribute of spin current is that it is associated with a flow of angular momentum, which is a vector quantity. This feature allows information to

be sent across nanoscopic structures. As opposed to charge current a spin current is invariant under time reversal. This property determines the low dissipative or even dissipativeless spin transport (Shen, 2008). Figs. 17a, b show the examples of spin currents calculated for AP configuration. Spin flip perturbation mixes the spin channels and therefore beyond the longitudinal current $\mathcal{I}^z$ also transverse currents appear. The observed minima or rapid change of spin currents occur near $V \sim 2\mathcal{R}$, what corresponds to maxima of AP transmission for this energy (compare Fig. 16a, b). Interesting observation is the occurrence of equilibrium spin current ($\mathcal{ESC}$). For the case discussed it is $\mathcal{I}^y$ component of spin current, which does not vanish for zero bias. The action of spin flip term is equivalent to the operation of magnetic field h_x in x-direction. Spin torque $h_x \times \sigma$ acts along y-axis, but is oriented in the opposite directions for right and left moving electrons. In consequence, the charge flow in opposite directions is associated with opposite y component of the spin. This happens in equilibrium, where charge current vanishes. Figures 17c, d illustrate that the magnitude and the sign of $\mathcal{ESC}$ is tunable by a gate voltage or magnetic field. It is worth to mention that the discussed system would also generate equilibrium spin current if only one ferromagnetic lead is connected to the dot with spin flips and such a system can be viewed as spin battery (Brataas et al., 2002; Hai et al., 2009). To supplement spin dependent transport characteristics we present on Fig. 18 spin-opposite shot noise. It characterizes the degree of correlations between charge transport events in opposite spin channels. In the absence of spin-flip scattering the currents of spin-up electrons and spin-down electrons are independent, and the cross-correlations between different spin-currents vanish. For simplicity we discuss only the case of parallel orientation of polarizations, when spin cross correlations are characterized by one element $\mathcal{S}_{L+L-}$. The positive values of $\mathcal{S}_{L+L-}$ means mutual amplification of currents in opposite spin

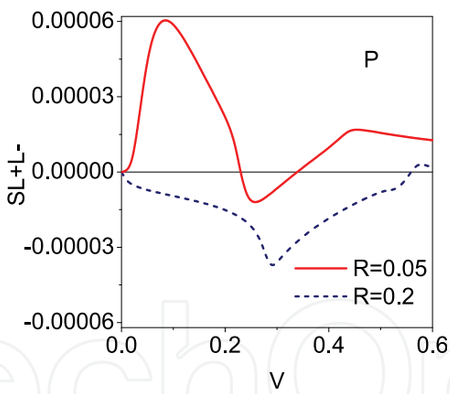


Fig. 18. Spin-opposite shot noise of CNT-QD for parallel orientation of polarizations of the leads $P = 0.6$, $E_0 = -5, \mathcal{U} = 15$.

channels and negative value their mutual weakening. Spin cross-correlations are determined by interference of spin rising and lowering transmissions, which are energy dependent. The decisive factors lowering shot noise is the Pauli exclusive principle and Coulomb interaction. These effects are in general case mixed. Pauli principle however acts only on electrons with the same spin and therefore spin-opposite noise probes interaction induced correlations only.

10. Conclusions

Carbon nanotubes present an ideal systems for spintronic applications due to long spin lifetimes and elaborated technology of coupling of them to ferromagnetic electrodes. The

domain sizes are much larger than electrode-nanotube interface and therefore CNTs are supposed to probe a single ferromagnetic domain. This allows for a precise spin control of transport through CNT-QD. Examining transport for different tunneling rates allows understanding of different transport regimes. For weak and intermediate transparency, strong correlations become decisive. Due to higher-order tunneling processes Kondo resonance is formed. This many-body resonance is much narrower than atomic or charge resonances and therefore transport control in this range requires much smaller effective fields. Disadvantage of working in this regime is necessity of use low temperatures. In carbon nanotubes however not only spin but also pseudospin is engaged resulting in highly symmetric SU(4) Kondo effect with considerably increased characteristic temperature. SU(4) Kondo effect is interesting, as the ground state involves a non-trivial entanglement of charge and orbital degrees of freedom. The description of this entanglement is not only a challenge for nanoscopic systems, important from application point of view, but its understanding sheds also a light on similar effects in bulk systems, where additional degeneracy results form crystal symmetry. In ideal semiconducting CNTs the orbital pseudospin and the real spin are indistinguishable, they start to differ in magnetic field. Studying quantum dots allows to analyze a rich aspects of Kondo physics owing to the tunability of relevant parameters of the dots and the ability for driving the system out of equilibrium in different ways.

The aim of this chapter was to give an overview of our current research on the impact of symmetry breaking perturbations on spin polarized transport in CNTs in the Kondo regime. We discussed the effect of magnetic field, polarizations of electrodes and real spin flip processes on the dot. The proposals of low field Kondo spin filter, Kondo spin valve and spin battery have been given. To supplement transport characteristics we have also presented short analysis of spin dependent shot noise. For spintronic devices, such as spin transistors it is necessary and beneficial to investigate the spin-current noise. In these devices, the spin currents rather than the charge currents are used as the carrier information. Investigation of spin-current noise has received very little attention up to now. Noise experiments are difficult to perform, since one needs to detect the shot noise over the background $1/f$ noise caused by fluctuations in the physical environment and measurement equipment. Relatively high Kondo temperature in CNTs is an advantage in possible measuring of shot noise in these systems, because high currents can be applied. To date, only one experiment on the noise in spin-orbital Kondo range of CNT-QD has been carried, and this result indicates that due to entanglement SU(4) Kondo systems remains noisy even in the unitary conductance limit (Delattre et al., 2009). There is still a lack of spin-resolved shot noise measurements, which are interesting because they give unambiguous probe of the electronic interactions. Such experiments seem to be within the reach of present-day measuring techniques, e.g. by spin filtering methods (Frolov et al., 2009), or detecting magnetization fluctuations. in the leads which senses the spin current noise via spin-transfer torque (Foros et al., 2005).

11. References

Averin, D. V. & Nazarov, Yu. V. (1992). *Single Charge Tunneling - Coulomb Blokade Phenomena in Nanostructures*, Plenum Press and NATO Scientific Affairs Division, New York

Babić, B., Kontos, T. & Schönenberger, C. (2004). Kondo effect in carbon nanotubes at half filling. *Phys. Rev. B*, 70, pp. 235419-1-9

Baibich, M. N., Broto J. M., Fert A., Nguyen Van Dau, F. & Petroff F., Etienne P., Creuzet, G., Friederich, A. & Chazelas J. (1988). Giant magnetoresistance of (001)Fe/(001)Cr Magnetic Superlattices. *Phys. Rev. Lett*, 61, pp. 2472-2475

Blanter, Ya. M. & Büttiker, M. (2000). Shot noise in mesoscopic conductors. *Phys. Rep.* 336, pp. 1-166

Binasch G., Grünberg, P., Saurenbach, F. & Zinn W. (1989). Enhanced magnetoresistance in layered magnetic structures with antiferromagnetic interlayer exchange. *Phys. Rev. B*, 39, pp. 4828-4830

Brataas, A., Tserkovnyak, Y., Bauer, G. E. W. & Halperin, B. I. (2002). Spin battery operated by ferromagnetic resonance. *Phys. Rev. B*, 66, pp. 060404-1-4

Buitelaar, M. R., Bachtold, A., Nussbaumer T., Iqbal, M. & Schönenberger, C. (2002). Multiwall carbon nanotubes as quantum dots. *Phys. Rev. Lett.*, 88, pp. 156801-1-4

Bułka, B. R. & Lipiński, S. (2003). Coherent electronic transport and Kondo resonance in magnetic nanostructures. *Phys. Rev. B*, 67, pp. 024404-1-8

Büsser, C. A. & Martins, G. B. (2007). Numerical results indicate a half-filling SU(4) Kondo state in carbon nanotubes. *Phys. Rev. B*, 75, pp. 045406-1-7

Choi, M. S., Sanchez, D. & Lopez, R. (2004). Kondo effect in a quantum dot coupled to ferromagnetic leads: A numerical renormalization group analysis. *Phys. Rev. Lett*, 92, pp. 056601-1-4

Choi, M., López, R., Aguado, R. (2005). SU(4) Kondo effect in carbon nanotubes. *Phys. Rev. Lett.* 95, pp. 067204-1-4

Cobden, D. H. & Nygård, J. (2004). Shell filling in closed single-wall carbon nanotube quantum dots. *Phys. Rev. Lett.*, 89, pp.046803-1-4

Coleman, P. (1987). Mixed valence as an almost broken symmetry. *Phys. Rev. B* 35, 5072-5116

Cottet, A. & Choi, M. S. (2006). Magnetoresistance of a quantum dot with spin-active interfaces. *Phys. Rev. B* 74, pp. 235316-1-9

Cottet, A., Kontos, T., Sahoo, S., Man, H. T., Choi, M. S., Belzig, W., Bruder, C., Morpurgo, A. F. & Schönenberger, C. (2006). Nanospintronics with carbon nanotubes. *Semicond. Sci. Technol.*, 21, pp. 78-95

Cronewett, S. M., Oesterkamp, T. H. & Kouwenhoven, L. P. (1998). A tunable Kondo effect in quantum dots. *Science* 291, pp. 540-544

Das Sarma, S. (2001). Spintronics. *American Scientist*, 89, pp. 516-523

De Franceschi, S., Hanson, R., van der Wiel, W. G., Elzerman, J. M., Wijpkema, J. J., Fujisawa, T., Tarucha, S. & Kouwenhoven (2002). Out-of-equilibrium Kondo effect in mesoscopic devices. *Phys. Rev. Lett.* 89, pp. 156801-1-4

de Haas, W. J, de Boer, J. & van den Berg G. J. (1933). The electrical resistance of gold, copper and lead at low temperatures. *Commun. Kamerlingh Onnes Lab.*, No. 233b; *Physica*, 1, pp. 1115-1124

Delattre, T., Feuillet-Palma, C., Herman, L. G., Morfin, P., Berroir, J. M., Fève, G., Plaçais, B., Glattli, D. C., Choi, M. S., Mora, C. & Kontos, T. (2009). Noisy Kondo impurities. *Nature Physics*, 5, pp. 208-212

Dresselhaus, M. S., Dresselhaus, G. & Avouris, Ph. (2001). *Carbon Nanotubes. Synthesis, Structure, Properties, and Applications*, Springer-Verlag, Berlin

Foros, J., Brataas, A., Tsevkovnyak, Y. & Bauer, G. E. W. (2005). Magnetization noise in magnetoelectronic nanostructures. *Phys. Rev. Lett.*, 95, pp. 016601-1-4

Frolov, S. M., Venkatesan, A., Yu, W., Folk, J. A. & Wegscheider, W. (2009). Electrical Generation of Pure Spin Currents in a Two-Dimensional Electron Gas. *Phys. Rev. Lett.* 102, pp. 116802-1-4

Galpin, M. R., Logan, D. E., Krishnamurthy, H. R. (2006). Dynamics of capacitively coupled double quantum dots. *J. Phys.: Condens. Matter*, 18, pp. 6571-6583

Galpin, M. R., Jayatilaka, F. W., Logan, D. E. & Anders F. B. (2010). Interplay between Kondo physics and spin-orbit coupling in carbon nanotube quantum dots. *Phys. Rev. B*, 81, pp. 075437-1-14

Goldhaber-Gordon, D., Shtrikman, H., Mahlul, D., Abuschmagder, D., Meiraev, U. & Kastner, M. A. (1998). Kondo effect in a single-electron transistor. *Nature* 391, pp. 156-159

Grobis, M., Rau, I. G., Potok, R. M., Shtrikman, H. & Goldhaber-Gordon, D. (2008). Universal scaling in nonequilibrium transport through a single channel Kondo dot. *Phys. Rev. Lett.*, 100, pp. 246601-1-4

Grove-Rasmussen, K., Jørgensen, H. J. & Lindelof, P. E. (2007). Fabry-Perot interference, Kondo effect and Coulomb blokade in carbon nanotubes. *Physica E*, 40, pp. 92-98

Hai, P. N., Ohya, S., Tanaka, M., Barnes, S. E. & Maekawa, S. (2009). Electromotive force and huge magnetoresistance in magnetic tunnel junctions. *Nature*, 458, pp. 489-492

Haldane, F. D. M. (1978). Scaling theory of the asymmetric Anderson Model. *Phys. Rev. Lett.*, 40, 416-419

Haug, H. & Jauho, A. P. (1998).*Quantum Kinetics in Transport and Optics of Semiconductors*, Springer, Berlin

Hauptmann, J. R., Paaske, J. & Lindelof, P. E. (2008). Electric-field-controlled spin reversal in a quantum dot with ferromagnetic contacts. *Nature Physics*, 4, pp. 373-376

Hewson, A. C. (1993). *The Kondo problem to heavy fermions*, pp.1-472, Cambridge University Press, ISBN 978-0521599474, Cambridge

Holleitner, A., Chudnovskiy, A., Pfannkuche, D., Eberl, K. & Blick R. H. (2004). Pseudospin Kondo correlations versus hybridized molecular states in double quantum dots. *Phys. Rev. B*, 70, pp. 075204-1-5

Iijima, S. (1991). Helical microtubules of graphitic carbon. *Nature*, 354, pp. 56-58

Iijima, S. & Ichihashi, T. (1993). Single-shell carbon nanotube of 1-nm diameter. *Nature*, 363, pp. 603-605

Jarillo-Herrero, P., Sapmaz, S., Dekker, C., Kouwenhoven, L. P. & van der Zant, H. S. J. (2004). Electron-hole symmetry in a semiconducting carbon nanotube quantum dot. *Nature*, 429, 389-392

Jarillo-Herrero, P., Kong, J., van der Zant, H. S. J., Dekker, C., Kouvenhoven, L. P. & De Franceschi, S. (2005). Orbital Kondo effect in carbon nanotubes. *Nature*, 434, pp. 484-488

Julliére, M. (1975). Tunneling between ferromagnetic films. *Phys. Rev. Lett.*, 54A, pp. 225-226

Kondo, J. (1964). Resistance minimum in dilute magnetic alloys. *Prog. Theor. Phys.*, 32, pp.37-49

Krychowski, D., Lipiński, S. & Krompiewski., S. (2007). Spin dependent transport through a carbon nanotube quantum dot in magnetic field. *J. Alloys and Compd.*, 442, pp. 379-381

Krychowski, D. & Lipiński, S. (2008). Tunnel magnetoresistance in carbon nanotube quantum dots. *Acta Phys. Pol. A*, 113, 545-548

Krychowski, D. & Lipiński, S. (2009). Kondo effect in carbon nanotube quantum dot in a magnetic field. *Acta Phys. Pol. A*, 115, pp. 293-29

Lacroix, C. (1998). Density of states for the Anderson model. *J. Phys. F: Metal Phys.*, 11, pp. 2389-2397

Langreth, D. C. (1966). Friedel sum rule for Anderson's model of localized impurity states. *Phys. Rev.*, 150, pp. 516-518

Liang, W., Bockrath, M., Bozovic, D., Hafner, J. H., Tinkham, M. & Park, H. (2001). Fabry-Perot interference in a nanotube electron waveguide. *Nature*, 411, pp. 665-669

Liang, W., Bockrath, M. & Park, H. (2002). Shell filling and exchange coupling in metallic single-walled carbon nanotubes. *Phys. Rev. Lett.*, 88, pp. 126801-1-4

Liang, W. J., Shores, M. P., Bockrath, M., Long, J. R. & Park (2002). Kondo resonance in a single-molecule transistor. *Nature* 417, pp. 725-729

Lim, J. S., Choi, M., Choi, M. Y., López, R. & Aguado, R. (2006). Kondo effect in carbon nanotubes: From SU(4) to SU(2) symmetry. *Phys. Rev. B* 74, pp. 205119-1-16

Lipiński, S. & Krychowski, D. (2005). Orbital Kondo effect and spin polarized transport through quantum dots. *Phys. Status. Solidi B* 242, pp. 206-209

Lipiński, S. & Krychowski, D. (2010). Spin-polarized current and shot noise in a carbon nanotube quantum dot in the Kondo regime. *Phys. Rev. B*, 81, pp. 115327-1-19

Loss, D. & DiVincenzo, D. P. (1998). Quantum computation with quantum dots. *Phys. Rev. A*, 57, 120-126

Makarowski, A., Zhukov, A., Liu, J. & Finkelstein, G. (2007). SU(2) amd SU(4) Kondo effect in carbon nanotube quantum dots. *Phys. Rev. B*, 75, 241407(R)-1-4

Martinek, J., Utsumi, Y., Imamura, H., Barnaś, J., Maekawa, S., König, J. & Schön, G. (2003). Kondo Effect in Quantum Dots Coupled to Ferromagnetic Leads. *Phys. Rev. Lett.* 91, pp. 127203-1-4

Martinek, J., Sindel, M., Borda, L., Barnaś, Bulla, R., König, J., Schön, G., Maekawa, S. & von Delft, J. (2005). Gate-controlled spin splitting in quantum dots with ferromagnetic leads in the Kondo regime. *Phys. Rev. B.*, 72, pp. 121302-1-4

Mizumo, M., Kim, E. H. & Martins G. B. (2009). Transport and strong-correlation phenomena in carbon nanotube quantum dots in a magnetic field. *J. Phys.: Condens. Matter* 21, pp. 292208-1-5

Ng, T. K. (1996). AC response in the nonequilibrium Anderson impurity model. *Phys. Rev. Lett.*, 76, pp. 487-490

Novoselov, K. S., Geim, A. K., Morozov, S. V., Jiang, D., Katsnelson, M. I., Grigorieva, I. V., Dubonos, S. V. & Frisov, A. A.(2005). Two-dimensional gas of massless Dirac fermions in graphene. *Nature*, 438, pp. 197-200

Nygård, J., Cobden, D. H. & Lindelof, P. E. (2000). Kondo physics in carbon nanotube. *Nature*, 408, pp. 342-346

Paaske, J., Rosch, A., Wölfe, P., Mason, N., Marcus, C. M. & Nygård, J. (2006). Non-equilibrium singlet-triplet KOndo effect in carbon nanotubes. *Nature Physics* 2, pp. 460-464

Park, J., Pasupathy, A. N., Goldsmith, J. I., Chang, C., Yaish, Y., Petta, J. R., Rinkoski, M., Sethna, J. P., Abruna, H. D., McEuen, P. L. & Ralph, D. C. (2002). Coulomb blokade and the Kondo effect in single-atom transistor. *Nature* 417, pp. 722-725

Sasaki, S., Amaha, S., Asakawa, N., Eto, M. & Tarucha S. (2004). Enhanced Kondo effect via tuned orbital degeneracy in a spin 1/2 artificial atom. *Phys. Rev. Lett.* 93, pp. 017205-1-4

Sergueev, N., Sun, Q. F., Guo, H., Wang, B. G. & Wang, J. (2002). Spin-polarized transport through a quantum dot: Anderson model with on-site Coulomb repulsion. *Phys. Rev. B*, 65, 165303-1-9

Shen, S. Q. (2008). Spintronics and spin current. *AAPPS Bulletin*, Vol. 18, No. 5, pp. 29-36

Świrkowicz, R., Wilczyński, M. & Barnaś, J. (2006). Spin-polarized transport through a single-level quantum dot in the Kondo regime. *J. Phys.: Condens. Matter.*, 18, pp. 2291-1-9

Tanaka, M. & Higo Y. (2001). Large tunneling magnetoresistance in GaMnAs/AlAs/GaMnAs ferromagnetic semicontuctor tunnel junction. *Phys. Rev. Lett.*, 87, pp. 026602-1-4

Wallace, P. R. (1947). The band theory of graphite. *Phys. Rev.*, 71, pp. 622-634

Wei, Ch., Cho K. & Srivastava D. (2003). Tensile strength of carbon nanotube under realistic temperature and strain rate. *Phys. Rev. B*, 67, pp. 115407-1-6

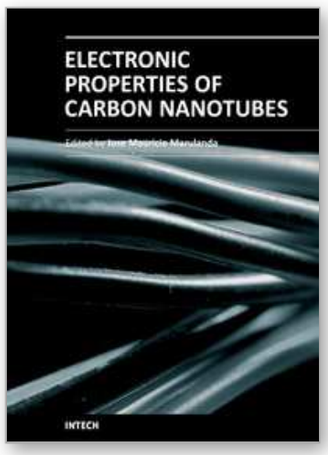
Wilhelm, U., Schmid, J., Weis, J. & v. Klitzing, K. (2002). Experimental evidance for spinless Kondo effect in two electrostically coupled quantum dot system. *Phisics E*, 14, pp. 385-390

Wu, F., Danneau, R., Queipo, P., Kauppinen, E., Tsuneta, T. & Hakonen, P. J. (2009). Single-walled carbon nanotube weak links in Kondo regime with zero-field splitting. *Phys. Rev. B*, 79, pp. 073404-1-4

Xiong, Z. H., Wu, D., Valy Vardeny, Z. & Shi, J. (2004). Giant magnetoresistance in organic spin-valves. *Nature*, 427, pp. 821-824

Žutić, I., Fabian, J. & Das Sarma, S. (2004). Spintronics: Fundamentals and applications. *Rev. Mod. Phys.*, 76, pp. 323-410

IntechOpen



Electronic Properties of Carbon Nanotubes

Edited by Prof. Jose Mauricio Marulanda

ISBN 978-953-307-499-3
Hard cover, 680 pages
Publisher InTech
Published online 27, July, 2011
Published in print edition July, 2011

Carbon nanotubes (CNTs), discovered in 1991, have been a subject of intensive research for a wide range of applications. These one-dimensional (1D) graphene sheets rolled into a tubular form have been the target of many researchers around the world. This book concentrates on the semiconductor physics of carbon nanotubes, it brings unique insight into the phenomena encountered in the electronic structure when operating with carbon nanotubes. This book also presents to reader useful information on the fabrication and applications of these outstanding materials. The main objective of this book is to give in-depth understanding of the physics and electronic structure of carbon nanotubes. Readers of this book should have a strong background on physical electronics and semiconductor device physics. This book first discusses fabrication techniques followed by an analysis on the physical properties of carbon nanotubes, including density of states and electronic structures. Ultimately, the book pursues a significant amount of work in the industry applications of carbon nanotubes.

How to reference

In order to correctly reference this scholarly work, feel free to copy and paste the following:

Stanislaw Lipinski and Damian Krychowski (2011). Spin Dependent Transport through a Carbon Nanotube Quantum Dot in the Kondo Regime, Electronic Properties of Carbon Nanotubes, Prof. Jose Mauricio Marulanda (Ed.), ISBN: 978-953-307-499-3, InTech, Available from: http://www.intechopen.com/books/electronic-properties-of-carbon-nanotubes/spin-dependent-transport-through-a-carbon-nanotube-quantum-dot-in-the-kondo-regime

INTECH
open science | open minds

InTech Europe
University Campus STeP Ri
Slavka Krautzeka 83/A
51000 Rijeka, Croatia
Phone: +385 (51) 770 447
Fax: +385 (51) 686 166
www.intechopen.com

InTech China
Unit 405, Office Block, Hotel Equatorial Shanghai
No.65, Yan An Road (West), Shanghai, 200040, China
中国上海市延安西路65号上海国际贵都大饭店办公楼405单元
Phone: +86-21-62489820
Fax: +86-21-62489821

© 2011 The Author(s). Licensee IntechOpen. This chapter is distributed under the terms of the Creative Commons Attribution-NonCommercial-ShareAlike-3.0 License, which permits use, distribution and reproduction for non-commercial purposes, provided the original is properly cited and derivative works building on this content are distributed under the same license.

IntechOpen

IntechOpen